



Comparative DEMS study on the electrochemical oxidation of carbon blacks

Sean J. Ashton, Matthias Arenz*

University of Copenhagen, Department of Chemistry, Universitetsparken 5, 2100 Copenhagen, Denmark

HIGHLIGHTS

- We quantitatively determine electrooxidation of carbon support materials.
- We can distinguish between the total and partial electrooxidation.
- Non or mildly heat treated carbon forms passivating layer.
- Heat treated carbons are less sensitive to oxidation–reduction cycles.

ARTICLE INFO

Article history:

Received 31 January 2012

Received in revised form

29 May 2012

Accepted 5 June 2012

Available online 13 June 2012

Keywords:

DEMS

Carbon oxidation reaction

PEM fuel cell

Carbon corrosion

Carbon supports

ABSTRACT

The intention of the study presented here is to compare the electrochemical oxidation tendencies of a pristine Ketjen Black EC300 high surface area (HSA) carbon black, and four graphitised counterparts heat-treated between 2100 and 3200 °C, such as those typically used as corrosion resistant carbon (CRC) supports for polymer electrolyte membrane fuel cell (PEMFC) catalysts. A methodology combining cyclic voltammetry (CV) and differential electrochemical mass spectrometry (DEMS) is used, which allows the characterisation and comparison of the complete electrochemical oxidation rates and behaviours of the various carbon blacks. It is observed that the behaviour of the carbon black towards electrochemical oxidation is highly dynamic, and dependent on the properties of the pristine carbon back, the degree of electrochemical oxidation and the potential pre-history. The behaviour of the non-graphitised and CRC samples graphitised ≤ 2450 °C suggests that electrochemical oxidation leads to the passivation of the carbon, which when reduced in a potential excursion to ≤ 0.24 V_{RHE} is lost allowing subsequent oxidation; however, CRC samples graphitised ≥ 2800 °C did not exhibit this same behaviour.

© 2012 Elsevier B.V. All rights reserved.

1. Introduction

The key aspects of polymer electrolyte membrane fuel cell (PEMFC) research and development are focused towards resolving issues concerning cost, efficiency and durability. In terms of durability, several processes such as PEM thinning, gas diffusion layer degradation, electrocatalyst (Pt) particle sintering and support corrosion have been found to contribute to the PEMFC performance deterioration [1], of which the latter two factors are directly related to the characteristics of the electrocatalyst material. These electrocatalysts typically consist of Pt nanoparticles that are finely dispersed on a high surface area (HSA) carbon black, which serve as almost ideal supports because of their high surface area, good electric conductivity and porosity. The standard electrode potential of 0.207 V_{RHE} for the complete oxidation of carbon to CO₂, however,

suggests that carbon is rather unstable in the PEMFC environment and inherently prone to electrochemical oxidation. Of particular concern is the number of start–stop events necessary in automotive PEMFC applications [2–7], during which the potential of the cathode may reach potentials up to 1.75 V_{RHE} [6] causing considerable quantities of CO₂ to be evolved [8] degrading the electrocatalyst and subsequently the performance of the PEMFC. A thorough fundamental understanding of the failure modes for each component in the development mitigating strategies to improve PEMFC endurance is therefore urgently required [1].

There are essentially two types of approach to the study of PEMFC degradation processes: (i) lifetime testing (LT) and (ii) accelerated stress testing (AST) [1,9]. LT involves operating the PEMFC as it is intended to be used, which although certainly provides the most reliable indication of durability is both time consuming and expensive with slow accumulation of data, whose interpretation is complicated by the wide range of parameters that can influence the long term durability of PEMFCs [10]. Consequently, AST is a considerably more popular approach to assessing

* Corresponding author. Tel.: +45 353 20002.

E-mail address: m.arenz@chem.ku.dk (M. Arenz).

PEMFC durability. These ASTs can take two forms, and involve either *in situ* or *ex situ* methodologies, similarly to the approach in assessing PEMFC electrocatalyst activities [11,12].

In situ AST methods typically involve fabricating an membrane electrode assembly (MEA) and subjecting it to specific treatments under controlled conditions that push the boundaries of the intended operating region of the PEMFC in order to stress and accelerate the degradation of the MEA components. In such experiments, the performance of the MEA is often monitored as a function of the AST parameter(s), such as current load, current load cycles or operating temperature [2,7,13–15]. The effect of the AST treatment on the MEA components may then be assessed by analysing the condition of the MEA after a degradation treatment [13,15–17], identifying process such as cathode thinning, Pt particle loss and Pt dissolution and re-precipitation [16,17]. There are also more sophisticated experiments which monitor corrosion processes online, for example, by measuring and correlating the CO₂ concentration in cathode PEMFC exhaust gas using FTIR spectroscopy [18,19] or sampled gas chromatography [7,14] with the deterioration in the PEMFC performance. Although undoubtedly essential, *in situ* AST methods are still relatively expensive and require the control of a large number of experimental variables (temperature, pressure, humidity etc.) and fabrication of the MEA. The screening of HSA electrocatalysts and/or corrosion resistant carbon (CRC) HSA catalyst support materials, as well as the precise elucidation of degradation processes to specific PEMFC components (whose deterioration may not be uniform but localised [15]) *in situ*, therefore, is by no means trivial.

A complementary approach using *ex situ* AST techniques is therefore valuable in order to enhance our fundamental understanding of the degradation processes of specific components. For example, studies using three-electrode electrochemical half cells have investigated the electrochemical oxidation of model carbons [20,21], carbon blacks [22–24] and HSA carbon supported Pt catalysts [22,25–29]. These studies typically involve applying a certain electrochemical treatment, using either CV [25,26,30], chronoamperometry [22] or potential pulse [22,31] perturbation to a potential of at least 1.2 V_{RHE}, with the intention of electrochemically oxidising the carbon or electrocatalyst material. The anodic electrode current observed is then often referred to as corrosion current [23] or it is assumed to correspond with the loss of carbon material [22]. The electrochemical AST treatment is then compared to a measurable property such as the apparent electrode double-layer capacitance [22] or the nature of the surface oxygen containing functional groups [31]. In electrochemical half-cell studies on HSA carbon supported Pt catalyst corrosion, however, the analysis of the electrode current is further complicated by the electrochemical reactions of the supported Pt particles, in particular the oxidation of the Pt surface > 0.74 V_{RHE} and the oxygen evolution reaction (OER) > 1.5 V_{RHE}. Using standard electrochemical half-cell methods therefore, it is impossible to decipher the carbon oxidation current based on the electrode current alone. Consequently, a measurable property of the electrocatalyst such as the electrochemical surface area (ECSA) of the supported Pt particles is often related to a parameter of the corrosion treatment, such as number of CVs [25,26,30], potential pulses [20] or potential hold time [22,32], analogous to *in situ* AST approaches. These methodologies have also been enhanced by utilising analytical techniques such as transmission electron microscopy (TEM) [25,26], secondary electron microscopy (SEM) [21], atomic force microscopy (AFM) [30,32], X-ray photoelectron microscopy (XPS) [20,30,32] and EQCM [24]. Alternatively, corrosion half-cell studies may also focus on the dissolution of pure Pt electrodes [33].

Standard *ex situ* electrochemical half-cell techniques are nevertheless limited to the clouded interpretation of a single

electrode current, even though a number of different electrochemical reaction processes are known to occur in the high potential regions > 1.2 V_{RHE}. Differential electrochemical mass spectrometry (DEMS) is therefore potentially very useful in the fundamental study of electrochemical oxidation processes by quantitatively measuring CO₂ and O₂, and has already been demonstrated in a handful of largely qualitative corrosion studies [34–36].

In the work presented here, we apply our recently developed methodology [37] which combines CV and DEMS in order to quantitatively characterise and compare the *ex situ* electrochemical oxidation tendencies of a pristine Ketjen Black EC300 HSA carbon black and four graphitised CRC counterparts that were heat-treated between 2100 and 3200 °C.

2. Experimental

The DEMS instrument is in principle of similar design to that reported previously [38]. It consists of a dual-cyclone thin-layer electrochemical flow cell, a microporous PTFE membrane (Gore, 0.03 µm pore size) interface, and a 3-stage differentially pumped high vacuum system including quadrupole mass spectrometer (QMS) (Pfeiffer Vacuum QMA 422). The counter electrode (CE) is positioned in a side-compartment of the thin-layer working electrode (WE) flow cell, located to the side of the cell inlet, whilst the reference electrode (RE) is located in a sealed compartment situated on the outlet of the flow cell. An electrolyte flow rate of 5 µL s⁻¹ through the thin-layer flow cell was maintained using a KDS 200 precision syringe pump (located on the flow outlet) withdrawing electrolyte from an Ar (purity 5.0) gas purged reservoir. In order to avoid potentiostat oscillation a stabilising resistor (~30 Ω) was added in series to the WE connection, and compensated for using a custom built negative impedance device (NID). The resulting uncompensated solution resistance (determined using AC voltammetry at 5 mV, 5000 Hz and 5 mV s⁻¹), typically ~10 Ω, was then corrected for during post measurement data treatment.

For the measurements, each carbon black stock suspension was prepared by ultrasonically dispersing the powdered sample in Millipore Milli-Q water to give solution concentration of 2.5 µg_c µL⁻¹ (EC300) and 4.3 µg_c µL⁻¹ (graphitised samples). Each measurement sample was then prepared by pipetting 20 µL of the stock suspension onto a mirror polished 5 mm Ø polycrystalline Au WE substrate and dried in air to provide a sample loading of 50 µg_c cm⁻² and 85 µg_c cm⁻², respectively. All experiments were performed at room temperature (295 K) in aqueous 0.5 mol dm⁻³ H₂SO₄ (Normaton; Merck, Germany) electrolyte prepared in Millipore Milli-Q water (<18.3 MΩ cm⁻¹, TOC < 5 ppb). The DEMS cell collection efficiency was determined prior to each experiment via a CO-stripping measurement on a polycrystalline Pt electrode, and the QMS was calibrated for CO₂ and O₂ at *m/z* = 44 and *m/z* = 32, respectively. The *I_{m/z=44}* and *I_{m/z=32}* mass ion currents were monitored online by the QMS, and the equivalent faradaic current (*I_f*) corresponding to the production of CO₂ and O₂ was calculated (assuming 4 e⁻ per molecule) using the respective calibration constants (2.95 and 1.65 C mol⁻¹) and measured cell collection efficiency (0.3 ± 0.02 at 5 µL s⁻¹). The remaining anodic current that could not be attributed to either the complete carbon oxidation reaction (COR) of the HSA carbon black (*I_{CO2}*), or the OER (*I_{O2}*) and polycrystalline Au background, is ascribed to the partial COR. All electrode potentials meanwhile are given with respect to the reversible hydrogen electrode (RHE) determined using the HOR/HER over polycrystalline Pt in hydrogen saturated electrolyte. The AST measurement procedure is presented in Section 3.2, which was performed after determining the capacitance of the sample.

3. Results and discussion

3.1. In situ method of determining carbon black sample loadings

In electrochemical experimentation on thin-film samples supported on a WE substrate it is often useful to be able to non-destructively determine the surface area (SA) and/or mass of the thin-film sample *in situ*. This allows the SA or mass of the electroactive material to be validated prior to the measurement in order to, for instance, avoid experimental errors that may arise from the sample preparation or the loss of the thin-film material, which is prone to detaching from the WE substrate when first submerged into electrolyte. While for HSA carbon supported Pt-based catalysts, the SA or mass of Pt may be non-destructively (and rather straightforwardly) determined by integrating the $H_{\text{ads}}/H_{\text{upd}}$ region or a CO-Stripping peak (using CO as a probe species); for non-Pt based materials that do not generally adsorb a probe species, the SA or mass determination of a sample *in situ* poses a more complex problem [39]. In this study, the mass of each of the HSA carbon black thin-film samples deposited on the WE substrate were characterised *in situ* using CV, the property of electrode capacitance and the predetermined gravimetric capacitance of the carbon material. This method is outlined for the Ketjen Black EC300 carbon in Fig. 1(A–C).

The largely featureless CV of Ketjen Black EC300 in Fig. 1(A), is almost rectangular in shape and appears to scale proportionally with the potential scan rate, both of which are characteristic of capacitive processes. The apparent double-layer capacitance of the electrode may then be extracted and plotted as a function of the electrode potential, as given in Fig. 1(B). A closer inspection reveals that the apparent capacitance does not remain completely constant over the whole potential range between 0.05 and 1.05 V_{RHE}, but instead possesses a minor parabolic relationship with the electrode potentials during the CV (ranging from 3.6 to 3.8 mF cm⁻²). This is furthermore slightly dependent upon the potential scan rate, converging at higher rates; an observation that may be related to distributed capacitance effects in porous electrodes [40,41]. In order to determine the gravimetric capacitance, the apparent double-layer capacitance at 0.25 V_{RHE} (substrate background subtracted) is plotted as a function of the sample loading on the WE substrate in Fig. 1(C). The electrode capacitance scales linearly within the applied range of thin-film sample loading for each carbon black, and the gravimetric capacitance for Ketjen Black EC300 is determined from the slope to be $61 \pm 4 \text{ F g}^{-1}$.

Details of the pre-determined gravimetric capacitances of all the carbon blacks examined in this study are given in Table 1, and compared with the BET areas and heat-treatment temperature. Using these values the sample loading of HSA carbon black material could be determined prior to experimentation by measuring the

Table 1

Details of the heat-treatment temperature, BET surface area, gravimetric and specific-double-layer capacitance of the pristine carbon black samples investigated.

Sample	Treatment temp./°C	BET area/m ² g ⁻¹	Gravimetric capacitance/F g ⁻¹	Capacitance per BET area/μF cm ⁻² _{BET}
EC300	—	720	61.2 ± 4	8.5
(GS-2100)	2100	247	14.1 ± 1	5.7
(GS-2450)	2450	230	10.6 ± 1	9.4
(GS-2800)	2800	218	7.5 ± 2	3.4
(GS-3200)	3200	135	8.5 ± 1	6.2

electrode capacitance of the thin-film sample, subtracting the WE substrate capacitance and comparing this to the pre-determined gravimetric capacitance.

In comparing the different carbons employed in this study (see Table 1) it is clear that the BET area of the EC300 carbon black ($720 \text{ m}^2 \text{ g}^{-1}$) is significantly larger than that of the heat-treated ($\leq 247 \text{ m}^2 \text{ g}^{-1}$) samples, which decreases further with increasing graphitisation temperature, particularly at 3200 °C ($135 \text{ m}^2 \text{ g}^{-1}$). This observation is roughly mirrored by the gravimetric capacitance, owing to the dependence of the double-layer capacitance on the surface area of the electrode, which in principle should (but not necessarily in practice) be rather independent of the electrode material and only on the surface area of the interface. The obtained (see Table 1) capacitance values normalised to the BET area are comparable to literature values that typically lie in the range of $4\text{--}10 \mu\text{F cm}^{-2}$ for a number of carbon blacks in various electrolytes [41,42]. More specifically, the $8.5 \mu\text{F cm}^{-2}$ observed for the EC300 carbon is closely comparable to the $8 \mu\text{F cm}^{-2}$ of Vulcan XC-72 [41]. In the practical application of this *in situ* method of validating the carbon mass of a thin-film, however, it is important to note that the scaling of the gravimetric capacitance with the carbon loading is prone to errors arising from the potentially significant influence of the WE substrate background. The substrate capacitance is of course ideally much smaller than that of the thin-film sample and must remain constant for reliable background subtraction. Materials with lower SA such as the graphitised CRCs (namely, those with BET areas $\leq 250 \text{ m}^2 \text{ g}^{-1}$) are therefore more susceptible to potentially significant errors.

3.2. AST measurement procedure using DEMS

The applied AST treatment was designed with the intention of comparing the electrochemical oxidation tendencies of the different carbon black samples using CV. Prior to the electrochemical oxidation treatment, the pristine samples were first characterised using CV between 0.05 and 1.0 V_{RHE} at various scan rates between 0.02 and 1.0 V s⁻¹. The potential of the WE was then stepped to 1.05 V_{RHE} in preparation for the electrochemical oxidation study on the HSA

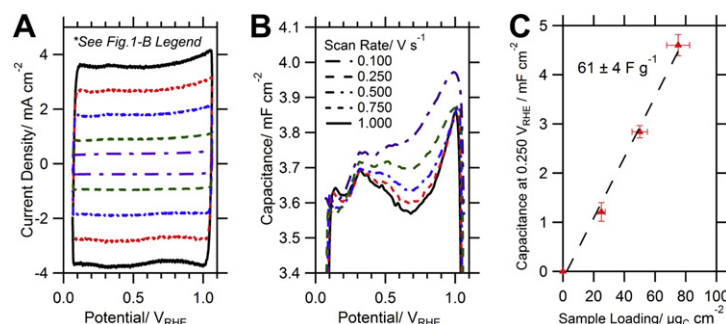


Fig. 1. (A) CV series of EC300 HSA carbon black recorded with various potential scan rates between 0.1 and 1.0 V s⁻¹ and (B) corresponding potential dependence of the double-layer electrode capacitance; (C) double-layer capacitance at 0.25 V_{RHE} plotted as a function of sample loading. All measurements were performed in Ar saturated 0.5 mol dm⁻³ H₂SO₄ electrolyte. From the slope of the linear fit (dashed curve (C)) a gravimetric capacitance of 61 F g^{-1} is determined for the EC300 HSA carbon black.

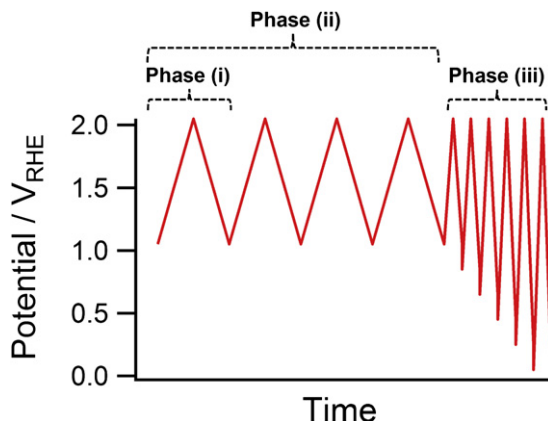


Fig. 2. Illustration of the AST experimental procedure used in the study. The procedure aims to reveal and compare the electrochemical oxidation tendencies of the HSA carbon black supports in three phases: (i) the initial oxidation, (ii) influence of repeated oxidation and (iii) influence of lower potential limit on subsequent oxidation.

carbon samples, which involved the comparison of three experimental phases (depicted in Fig. 2): phase (i) involves comparing the initial CV of the electrochemical oxidation to 2.05 V_{RHE} at 5 mV s⁻¹; phase (ii) investigates the progressive oxidation tendencies in four CVs between 1.05 and 2.05 V_{RHE}; phase (iii) investigates the influence of the lower potential limit which is progressively decreased from 1.05 to 0.05 V_{RHE} (in 200 mV steps) on the subsequent CV to 2.05 V_{RHE} at 20 mV s⁻¹.

3.2.1. Comparison of the initial electrochemical oxidation rates of the pristine carbon black samples (phase (i))

In order to reveal the differences in the initial electrochemical oxidation tendencies of the HSA carbon black samples using DEMS and CV, an initial comparison between the HSA carbons was made upon the very first high potential excursion (phase (i)) from 1.05 to 2.05 V_{RHE} at 5 mV s⁻¹. The trend of decreasing electrochemical oxidation rates with increasing graphitisation temperature, and decreasing SA observed is demonstrated in Fig. 3(A), which shows the comparison between the linear sweep voltammogram (LSV) and the respective current contributions determined from the concomitant mass spectrometry of the pristine EC300, the samples graphitised at 2100 °C and 3200 °C. It is observed that for all

samples, the faradaic electrode current coincides with the complete COR to CO₂ (I_{CO_2}). The small peak at ~1.4 V_{RHE} and the O₂ observed at potentials >1.7 V_{RHE}, meanwhile, can for almost all samples be solely attributed to the Au surface oxidation and OER on the polycrystalline Au substrate respectively, with the exception of the pristine EC300 where some additional O₂ is observed during the initial LSV. Finally, the overlap of the O₂ evolved in the OER on the polycrystalline Au substrate for heat-treated sample demonstrate the precision and reproducibility of the DEMS measurement.

The polycrystalline Au substrate background and quantity of CO₂ and O₂ produced, however, are insufficient to account for the whole of the faradaic electrode current. Consequently, the remaining faradaic electrode current is attributed to the partial COR of the carbon black. The partial COR may proceed via the oxidation of carbon to either oxygen containing functional groups or CO, and has been long understood to occur in conjunction with the complete COR to CO₂ [41].

The trend in both the mass and BET area normalised complete and partial COR charges (evolved during the initial CV) is shown in Fig. 3(B). The partial COR charge is observed to dominate the complete COR charge for the mildly graphitised (≤ 2450 °C) and, in particular, pristine EC300 carbon black samples, whereas for the more heavily graphitised samples the respective charges appear to be more comparable. The difference between the mass normalised charge evolved to CO₂ on the EC300 (0.06 C cm⁻²) and the graphitised counterparts (> 0.009 C cm⁻²) is significant (although by normalising these charges to BET the difference diminishes slightly) and we can conclude that the COR rate for the non-graphitised EC300 and mildly graphitised carbon (2100 °C) is clearly not SA dependent with respect to the more graphitised CRC samples.

In the logarithmic current vs. potential plots inset into Fig. 3(A), we are able to precisely evaluate both the potential at which CO₂ is first measured (using this particular DEMS instrument) and the slope of the linear Tafel region for the I_{CO_2} observed during the oxidation of each of the HSA carbon blacks, although in general these regions cover less than one decade of current. The CO₂ detection limit potentials, equivalent to 150 ppt, along with the Tafel-slopes extracted from the observed I_f , I_{CO_2} and $I_{Partial-Oxidation}$ are summarised in Table 2.

In this table we see that the CO₂ detection limit potential for the complete COR of the carbon blacks increases with increasing heat-treatment temperature, with clear steps between the EC300, the

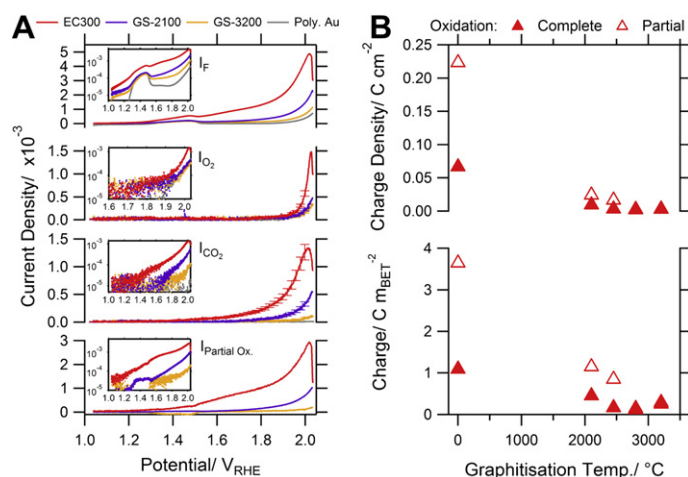


Fig. 3. (A) Comparison of the CV, I_{O_2} , I_{CO_2} and $I_{Partial-Oxidation}$ of the pristine HSA carbon black supports (EC300, GS-2100 and GS-3200) during the initial potential excursion to 2.05 V_{RHE} (phase (i)) of the electrochemical oxidation treatment (note that the polycrystalline Au substrate background is shown for reference). The insets show the corresponding data plotted in logarithmic (current) scale. (B) Resulting charges for the complete (solid markers) and partial (hollow markers) electrochemical oxidation of the HSA carbon black samples normalised to 85 $\mu\text{g}_c \text{cm}^{-2}$.

Table 2

Details of the CO_2 detection limit (150 ppt) potential and Tafel slopes for the I_f , I_{CO_2} and $I_{\text{Partial-Oxidation}}$ currents extracted from the initial electrochemical oxidation excursion to 2.05 V_{RHE} for the HSA carbon black samples. Tafel slopes marked * were fitted $<1.8 V_{\text{RHE}}$.

Sample	Graphitisation temp./°C	CO ₂ detection limit potential/V _{RHE}	Tafel-slope/mV Dec ⁻¹		
			I_f	I_{CO_2}	$I_{\text{Partial-Ox}}$
EC300	–	1.35	286 *413 ± 6 229 ± 2		367
(GS-2100)	2100	1.68	241 *307 ± 11 170 ± 2		292
(GS-2450)	2450	1.84	228	200 ± 9	208
(GS-2800)	2800	1.88	220	206 ± 11	–
(GS-3200)	3200	1.93	219	170 ± 9	–

mildly graphitised sample (2100°C), and the remaining graphitised samples ($>2450^{\circ}\text{C}$). In particular, the onset of the complete COR of the pristine EC300 and graphitised sample 4 (2100°C) determined to be 1.35 and $1.68 V_{\text{RHE}}$ respectively, are well within the potential window of a fuel cell cathode (i.e. up to $1.75 V_{\text{RHE}}$ during start–stop conditions [6]). In contrast, the onset of the complete COR of the remaining pristine, graphitised CRC samples ($\geq 2450^{\circ}\text{C}$) were observed to be somewhat higher ($\geq 1.84 V_{\text{RHE}}$) at the detection limit of our DEMS instrument. For the EC300 and GS-2100 carbons two different Tafel-slope linearities are observed in the logarithmic plot, above and below $1.8 V_{\text{RHE}}$. Below $1.8 V_{\text{RHE}}$ the slopes are comparatively shallow ($\geq 307 \text{ mV Dec}^{-1}$); whereas above $1.8 V_{\text{RHE}}$ the Tafel-slopes for all the carbon black samples are steeper ($\sim 200 \pm 30 \text{ mV Dec}^{-1}$) with no clear relationship between Tafel-slope and the heat-treatment temperature. Although we can extract these Tafel-esque slopes and detection limits, their implication is not entirely clear because the extraction of kinetic coefficients and extrapolation or rates assumes that the properties of the carbon surface remain constant i.e. it assumes that the behaviour of the carbon does not change as a result of the measurement, which we will see in phases (ii) and (iii) is simply not the case.

3.2.2. Influence of repeated electrochemical oxidation to $2.05 V_{\text{RHE}}$ of the carbon black samples (phase (ii))

In order to assess the changes that occur in the respective electrochemical COR tendencies upon repeated voltage cycling, a further three high potential CVs were performed between 1.05 and $2.05 V_{\text{RHE}}$ in phase (ii) of the electrochemical oxidation experiment. An example series for the GS-2100 carbon is presented in Fig. 4(A), which shows that the complete COR to CO_2 progressively increased slightly in the first three CVs before decreasing again in the final fourth CV. The partial COR charge, however, remained comparatively consistent whilst no significant changes in the Tafel-esque slopes were observed (see inset of Fig. 4A). With the intention of revealing and summarising the trends in phase (ii) more quantitatively, the electrode charge evolved that is attributed to the complete and partial COR processes during each of the first four CVs are plotted for the respective carbons as a function of the cumulative complete COR charge in Fig. 4(B)–(F). By viewing the data in this way we are able to bring greater focus onto the influence of the pre-history of the samples, i.e. the dependence of the partial and complete COR processes on the prior oxidation of the carbon black sample.

The repeated oxidation of the EC300 and heat-treated CRC counterparts reveals three trends in the electrochemical oxidation tendencies of carbon blacks, which is in turn related to the heat-treatment temperature and therefore degree of graphitisation. For the pristine EC300 sample (Fig. 4(B)), the electrochemical oxidation ceased abruptly following the first potential sweep, a process that has been previously attributed to the passivation of the carbon surface by non-electrochemically oxidisable oxygen-containing surface functional groups [37]. In contrast, the oxidation of the mildly heat-treated (2100°C) carbon progressively increases during the first three CVs before decreasing in the final fourth CV (Fig. 4(A) and (C)). The electrochemical oxidation of all remaining CRC samples heat-treated at $T \geq 2450^{\circ}\text{C}$ meanwhile progressively increases for each of the first four CVs (Fig. 4(D)–(F)). In all cases the complete COR is accompanied by the partial COR, and all O_2 observed is again attributed to the OER on polycrystalline Au

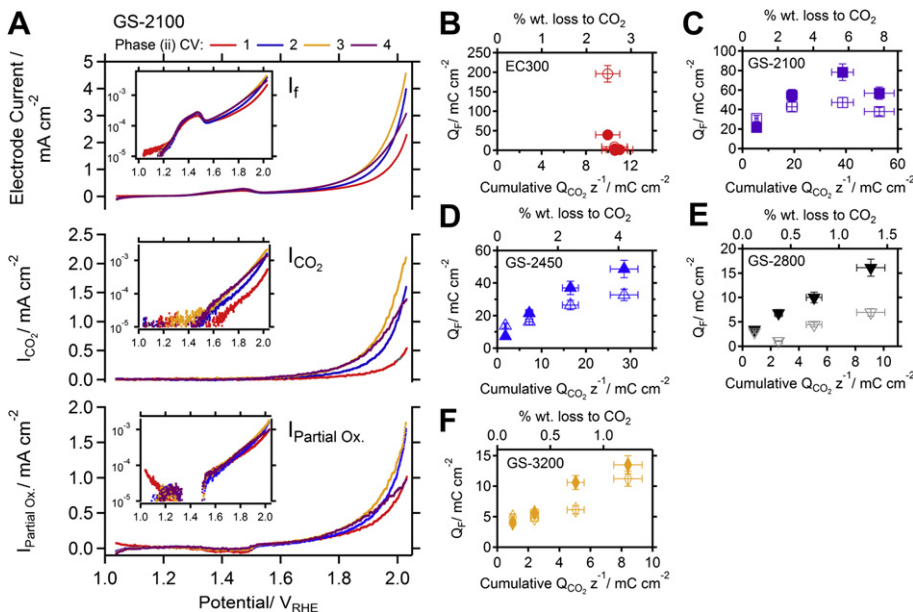


Fig. 4. (A) LSVs and corresponding I_{CO_2} and $I_{\text{Partial-Oxidation}}$ for phase (ii) of the electrochemical AST procedure of GS-2100 $^{\circ}\text{C}$ in Ar saturated $0.05 \text{ mol dm}^{-3} \text{ H}_2\text{SO}_4$, 5 mV s^{-1} . The insets show the corresponding data plotted in logarithmic (current) scale. (B–F) Resulting complete (solid markers) and partial (hollow markers) electrochemical oxidation charges of the respective HSA carbon blacks evolved during each CV in phase (ii) of the AST procedure. The oxidation charges are plotted as a function of the cumulative CO_2 charge evolved in order to bring focus onto the significance of each CV.

substrate. At this point in the electrochemical oxidation treatment, the percentage weight loss of carbon (due to complete COR to CO_2) follows the order: GS-2100 > 2450 > EC300 > 2800–3200 °C, in contrast to the charge evolved during the initial potential excursion where EC300 oxidised to the most extent. Before rationalising these three trends, it is useful to evaluate the influence of the lower electrode potential limit in phase (iii) of the experiment.

3.2.3. Influence of the lower potential limit on the subsequent electrochemical oxidation of the electrochemically oxidised carbon black samples (phase (iii))

In phase (iii) of the electrochemical oxidation experiment, the effect of the lower electrode potential limit (i.e. the reduction of the carbon), on the COR of the now oxidised (in phases (i) and (ii)) carbon blacks was investigated. Here, the lower potential limit was

progressively decreased from 1.05 V_{RHE} (lower limit in phase (ii)) to 0.05 V_{RHE} in steps of 200 mV. The sequence of CVs demonstrating the significant influence that lowering the electrode potential to ≤ 0.25 V_{RHE} has on the subsequent electrochemical oxidation are summarised in Fig. 5(A)–(C) for the pristine EC300, 2100 °C and 3200 °C samples, respectively.

The effect of the reduction of the oxidised carbon surface on the subsequent COR can again be categorised into three trends. By decreasing the WE potential to 0.05 V_{RHE} and reducing the EC300 HSA carbon black (Fig. 5(A)), we observe that the quantity of electrochemical oxidation current that occurs during the subsequent positive high potential sweep is not only significant, but also begins at the considerably lower potential of ~0.5 V_{RHE} peaking at ~1.7 V_{RHE}. The electrochemical oxidation of the mildly graphitised samples heat-treated ≤ 2450 °C (Fig. 5(B)) meanwhile, appears to be

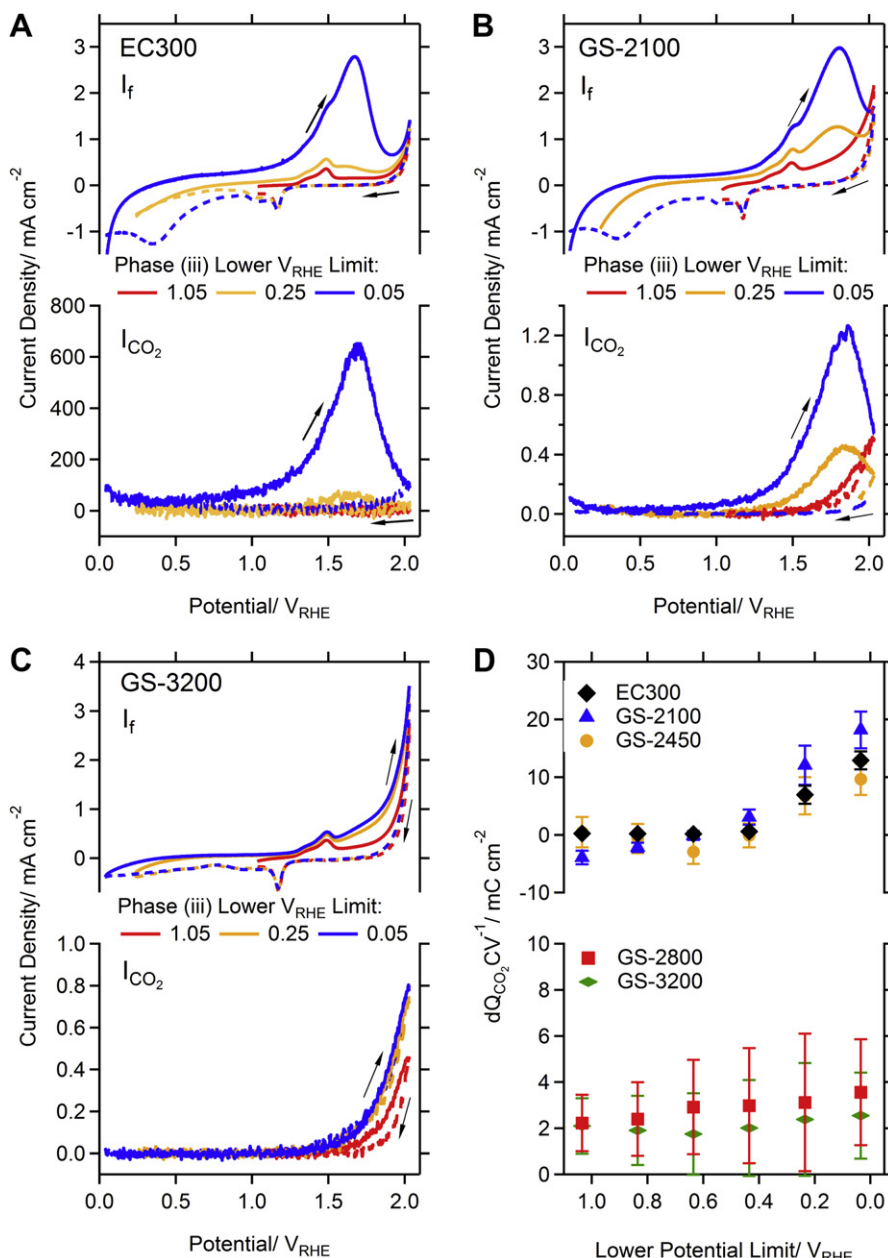


Fig. 5. (A–C) Comparison of CVs of the electrochemical oxidative of the HSA carbon black samples [(A) EC300, (B) GS-2100 °C, and (C) GS-3200 °C] during phase (iii) of the experiment (note that only CVs with the lower limits of 1.05, 0.205 and 0.05 are shown for simplicity). (D) The differential complete COR charge plotted as a function of the lower potential limit. By decreasing the lower potential limit to ≤ 0.24 V_{RHE} the oxidation of the HSA carbon black can be reinitiated (A) or significantly enhanced (B).

enhanced by decreasing the lower electrode potential limit to ≤ 0.24 V_{RHE} exhibiting the same broad peak feature at 1.7 V_{RHE}. Furthermore, the reduction of the HSA carbon black seemingly coincides with a non-oxidative discharge of CO₂ at potentials below the standard redox potential < 0.207 V_{RHE} of the complete COR. In contrast to the profound effect that the electrochemical reduction of the EC300 and mildly heat-treated ≤ 2450 °C carbon blacks had on the subsequent partial and complete COR to CO₂, the samples heat-treated ≥ 2800 °C are comparatively unaffected by the lower electrode potential (Fig. 5(C)). In order to bring greater focus on the influence of the lower electrode potential limit on the quantity of subsequent oxidation, the differential complete COR charge ($\delta Q/\delta CV$) for each subsequent CV is plotted as a function of the lower electrode potential limit in Fig. 5(D). This plot clearly shows that by decreasing the lower electrode potential limit to ≤ 0.24 V_{RHE}, the complete COR charge increases significantly in the subsequent CV on the EC300 and mildly heat-treated (2100–2450 °C) samples while the electrochemical COR processes of the CRC samples treated at higher temperatures (> 2800 °C) remain uninfluenced. The subsequent increase in the electrochemical oxidation is attributed to the destruction of the passivating, non-electrochemically oxidisable surface functional groups that form during the initial oxidation processes (in phases (i) and (ii)).

3.3. Overall consequences of the electrochemical oxidation treatment

The total quantity of the complete and partial COR charges evolved during the whole (phases (i)–(iii)) electrochemical oxidation treatment of each sample, is summarised as a function of the heat-treatment temperature in Fig. 6.

The complete COR of the graphitised HSA carbon supports resulted in a carbon weight loss of between 10 and 4wt.% with generally higher resistance observed for the more heavily graphitised samples. The ratios of the complete to the partial COR charges on the graphitised samples are $\sim 1:1$. The carbon weight loss of the non-graphitised EC300 carbon black to CO₂ was overall comparable to the more heavily graphitised samples. When normalised to the BET area of the samples, the specific complete COR charge evolved from the EC300 is in fact less than half that of the most graphitised materials (≥ 2800 °C), in stark contrast to the observations in Fig. 2(B) following phase (i).

3.4. Rationalisation of the observed electrochemical oxidation tendencies of carbon blacks

Although there is no commonly accepted description of the mechanism(s) describing the COR processes, previous work has stressed the importance of the oxygen containing surface functional groups on both the initial and long-term reactivity of the carbon blacks [23,41]. Often, the initial COR rates have been found to correlate positively with the oxygen content (i.e. the initial concentration of oxygen containing surface functional groups) of the pristine carbon black sample, whereas various terms such as phase-, protective-, stable-, or surface-oxide, oxide intermediates and complexes, have been used to try and describe the apparent influence of more stable oxygen containing surface functional groups on the COR during the course of an experiment (see discussion and references in Ref. [23]). It has been previously proposed that ‘many of the apparently contradictory results and interpretations (either electrochemical or gas phase oxidation studies prior to 1989) could be reconciled by invoking the relative stability of these oxides as the main discriminating factor’ going further to state that ‘the more stable oxides might play the role of decreasing the active surface area (ASA) of the carbon’ whereas ‘the

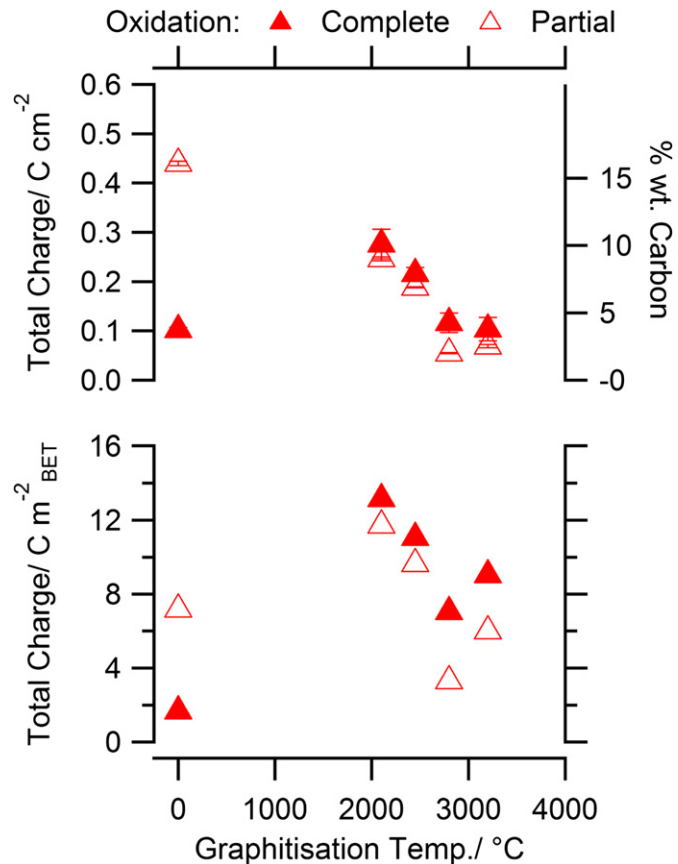


Fig. 6. (A) The total quantity of complete (solid markers) and partial (hollow markers) electrochemical oxidation charge evolved [during phases (i)–(iii)] for each HSA carbon sample plotted as a function of the graphitisation temperature. (B) Corresponding oxidation charges normalised to BET area.

formation of each product molecule, CO or CO₂, is accompanied by the regeneration of a free site and subsequent formation of another complex [23] citing Refs. [43,44]. It is this approach to considering the relative stability of the oxygen containing surface functional groups formed, and their influence on the electrochemically oxidisable surface area (EOSA) of the carbon that can be used to rationalise the trends observed in this study.

The initial rate of the COR processes on the carbon black can be expected to be determined by the nature and concentration of the electrochemically oxidisable surface functional groups that act as nucleation sites for either the complete oxidation to CO₂, or partial oxidation to either CO or surface oxygen containing functional group(s), i.e. they define the EOSA of the carbon. If we consider that the COR to either CO₂ or CO must involve the breakage of one or more C–C bonds, which will in-turn deteriorate the microstructure of the carbon generating at least one new active site, then these COR processes can be considered to either maintain or increase the EOSA (unless of course the carbon microstructure is completely consumed). Alternatively, if the partial COR proceeds to form oxygen containing surface functional group(s) that are stable (i.e. non-electrochemically oxidisable), then any further oxidation to CO₂ or CO will cease at this site, effectively decreasing the EOSA.

4. Conclusions

The intention of the study presented here was to investigate and compare the electrochemical oxidation tendencies of a pristine HSA carbon black, and four graphitised CRC counterparts heat-treated

between 2100 and 3200 °C, which may be used as supports for polymer electrolyte membrane fuel cell catalysts. A methodology was demonstrated which combines CV and DEMS that allows the characterisation and comparison of the electrochemical oxidation rates and tendencies of the various carbon blacks. It was observed that the behaviour of the carbon black towards electrochemical oxidation is highly dependent on the properties of the pristine carbon black and the degree of electrochemical oxidation, which is furthermore dynamic. During the very first high potential excursion, the complete oxidation of the pristine EC300 and GS-2100 sample to CO₂ (observed at 1.35 and 1.68 V_{RHE} respectively) occurs well within the operating limits of the fuel cell cathode (during stop–start), whereas no CO₂ was observed below 1.84 V_{RHE} for the remaining graphitised samples (≥ 2450 °C). Our observations, however, indicate that the oxidation of the carbon can significantly change its subsequent behaviour towards further oxidation as the EOSA of the carbon changes. Furthermore, by reducing the oxidised carbon black at potentials of ≤ 0.24 V_{RHE} the electrochemical oxidation may be re-initiated or enhanced for the pristine or mildly graphitised (≤ 2450 °C) carbon black samples (evolving CO₂ at potentials as low as 0.5 V_{RHE}) whereas the more heavily graphitised CRC samples (≥ 2800 °C) were seemingly unaffected. This behaviour can be rationalised by considering the tendency of each carbon to form passivating non-electrochemically oxidisable surface functional group(s), which when reduced is lost, allowing significant further electrochemical oxidation to occur. Thus, the apparently contradictory results and interpretations found in fuel cell AST literature may in part be due to different pre-conditions during testing. Furthermore, these findings indicate that the large differences observed between fuel cell steady state and potential cycling AST are not only related to the behaviour of supported Pt particles but also to the carbon support itself. Concerning the role of Pt, and in light of the apparently significant partial carbon oxidation current we observed, it should be emphasised that there is a crucial difference between (i) Pt catalysing the corrosion of carbon, and (ii) Pt catalysing the oxidation of carbon corrosion products, such as CO.

Overall, the methodology presented here revealed clear trends in the electrochemical oxidation behaviour of the different carbon blacks, offering new insights into their behaviour opening up future corrosion studies on other electrocatalyst support materials, and HSA carbon supported Pt catalysts using DEMS.

Acknowledgements

This work was supported by the German DFG through the Emmy-Noether project ARE852/1-1 and the Danish DFF through grant# 10-081337. We thank Z. Jusys from the University of Ulm for the many fruitful discussions concerning DEMS.

References

- [1] S. Zhang, X.-Z. Yuan, J.N.C. Hin, H. Wang, K.A. Friedrich, M. Schulze, *Journal of Power Sources* 194 (2009) 588–600.
- [2] H.R. Haas, M.T. Davis, *ECS Transactions* 25 (2009) 1623–1631.
- [3] J.P. Meyers, R.M. Darling, *Journal of the Electrochemical Society* 153 (2006) A1432–A1442.
- [4] C.A. Reiser, L. Bregoli, T.W. Patterson, J.S. Yi, J.D. Yang, M.L. Perry, T.D. Jarvis, *Electrochemical and Solid-State Letters* 8 (2005) A273–A276.
- [5] J. Kim, J. Lee, Y. Tak, *Journal of Power Sources* 192 (2009) 674–678.
- [6] H. Tang, Z. Qi, M. Ramani, J.F. Elter, *Journal of Power Sources* 158 (2006) 1306–1312.
- [7] P.T. Yu, W. Gu, R. Makharia, F.T. Wagner, H. Gasteiger, *ECS Transactions* 3 (2006) 797–809.
- [8] W.R. Baumgartner, P. Parz, S.D. Fraser, E. Wallnöfer, V. Hacker, *Journal of Power Sources* 182 (2008) 413–421.
- [9] R. Borup, J. Meyers, B. Pivovar, Y.S. Kim, R. Mukundan, N. Garland, D. Myers, M. Wilson, F. Garzon, D. Wood, P. Zelenay, K. More, K. Stroh, T. Zawodzinski, J. Boncella, J.E. McGrath, M. Inaba, K. Miyatake, M. Hori, K. Ota, Z. Ogumi, S. Miyata, A. Nishikata, Z. Siroma, Y. Uchimoto, K. Yasuda, K.I. Kimijima, N. Iwashita, *Chemical Reviews* 107 (2007) 3904–3951.
- [10] W. Schmittinger, A. Vahidi, *Journal of Power Sources* 180 (2008) 1–14.
- [11] H.A. Gasteiger, S.S. Kocha, B. Sompalli, F.T. Wagner, *Applied Catalysis B-Environmental* 56 (2005) 9–35.
- [12] K.J.J. Mayrhofer, D. Strmcnik, B.B. Blizanac, V. Stamenkovic, M. Arenz, N.M. Markovic, *Electrochimica Acta* 53 (2008) 3181–3188.
- [13] T. Yoda, H. Uchida, M. Watanabe, *Electrochimica Acta* 52 (2007) 5997–6005.
- [14] H.A. Gasteiger, W. Gu, B. Litteer, R. Makharia, B. Brady, M. Budinski, E. Thompson, F.T. Wagner, S.G. Yan, P.T. Yu, in: S. Kakaç, A. Pramanick, L. Vasiliev (Eds.), *Mini-Micro Fuel Cells*, Springer, Netherlands, 2008, pp. 225–233.
- [15] T.W. Patterson, R.M. Darling, *Electrochemical and Solid-State Letters* 9 (2006) A183–A185.
- [16] S. Chen, H.A. Gasteiger, K. Hayakawa, T. Tada, Y. Shao-Horn, *Journal of the Electrochemical Society* 157 (2010) A82–A97.
- [17] J. Zhang, B.A. Litteer, W. Gu, H. Liu, H.A. Gasteiger, *Journal of the Electrochemical Society* 154 (2007) B1006–B1011.
- [18] S. Maass, F. Finsterwalder, G. Frank, R. Hartmann, C. Merten, *Journal of Power Sources* 176 (2008) 444–451.
- [19] C. Mei, M.S. Ruthkosky, B. Merzouguia, S. Swathirajan, M.P. Balogh, S.H. Oh, *Investigation of Thermal and Electrochemical Degradation of Fuel Cell Catalysts*, Elsevier, Amsterdam, 2006.
- [20] M. Nose, T. Kinumoto, H.S. Choo, K. Miyazaki, T. Abe, Z. Ogumi, *Fuel Cells* 9 (2009) 284–290.
- [21] T. Kinumoto, K. Takai, Y. Iriyama, T. Abe, M. Inaba, Z. Ogumi, *Journal of the Electrochemical Society* 153 (2006) A58–A63.
- [22] S.C. Ball, S.L. Hudson, D. Thompsett, B. Theobald, *Journal of Power Sources* 171 (2007) 18–25.
- [23] P.L. Antonucci, L. Pino, N. Giordano, G. Pinna, *Materials Chemistry and Physics* 21 (1989) 495–506.
- [24] C.-C. Hung, P.-Y. Lim, J.-R. Chen, H.C. Shih, *Journal of Power Sources* 196 (2011) 140–146.
- [25] K.J.J. Mayrhofer, J.C. Meier, S.J. Ashton, G.K.H. Wiberg, F. Kraus, M. Hanzlik, M. Arenz, *Electrochemistry Communications* 10 (2008) 1144–1147.
- [26] K.J.J. Mayrhofer, S.J. Ashton, J.C. Meier, G.K.H. Wiberg, M. Hanzlik, M. Arenz, *Journal of Power Sources* 185 (2008) 734–739.
- [27] K. Hartl, M. Hanzlik, M. Arenz, *Energy & Environmental Science* 4 (2011) 234–238.
- [28] K. Schlogl, K.J.J. Mayrhofer, M. Hanzlik, M. Arenz, *Journal of Electroanalytical Chemistry* 662 (2011) 355–360.
- [29] F.J. Perez-Alonso, C.F. Elkjaer, S.S. Shim, B.L. Abrams, I.E.L. Stephens, I. Chorkendorff, *Journal of Power Sources* 196 (2011) 6085–6091.
- [30] H.S. Choo, T. Kinumoto, M. Nose, K. Miyazaki, T. Abe, Z. Ogumi, *Journal of Power Sources* 185 (2008) 740–746.
- [31] B. Avasarala, R. Moore, P. Haldar, *Electrochimica Acta* 55 (2010) 4765–4771.
- [32] H.-S. Choo, T. Kinumoto, S.-K. Jeong, Y. Iriyama, T. Abe, Z. Ogumi, *Journal of the Electrochemical Society* 154 (2007) B1017–B1023.
- [33] F. Kodera, Y. Kuwahara, A. Nakazawa, M. Umeda, *Journal of Power Sources* 172 (2007) 698–703.
- [34] L.C. Colmenares, A. Wurth, Z. Jusys, R.J. Behm, *Journal of Power Sources* 190 (2009) 14–24.
- [35] J. Willsau, J. Heitbaum, *Journal of Electroanalytical Chemistry* 161 (1984) 93–101.
- [36] L. Ming-fang, T. Qian, L. Ling-wen, X. Jie, C. Jun, C. Yan-xia, *Chinese Journal of Chemical Physics* 23 (2010) 442.
- [37] S.J. Ashton, M. Arenz, *Electrochemistry Communications* 13 (2011) 1473–1475.
- [38] Z. Jusys, H. Massong, H. Baltruschat, *Journal of the Electrochemical Society* 146 (1999) 1093–1098.
- [39] G.K.H. Wiberg, K.J.J. Mayrhofer, M. Arenz, *Fuel Cells* 10 (2010) 575–581.
- [40] S. Trasatti, O.A. Petrii, *Journal of Electroanalytical Chemistry* 327 (1992) 353–376.
- [41] K. Kinoshita, *Carbon – Electrochemical and Physicochemical Properties*, Wiley, 1987.
- [42] O. Barbieri, M. Hahn, A. Herzog, R. Kötz, *Carbon* 43 (2005) 1303–1310.
- [43] N.R. Laine, F.J. Vastola, P.L. Walker Jr., *Journal of Physical Chemistry* (1963).
- [44] S. Ahmed, M.H. Back, *Carbon* 23 (1985).